

Quantum feedback algorithms for DNA assembly using FALQON variants

Pedro M. Prado,¹ Lucas A. M. Rattighieri,² Rafael Simões do Carmo,¹ Giovanni S. Franco,¹ Guilherme E. L. Peixe,¹ Alexandre Drinko,³ Erick G. Dorlass,³ Tatiana F. de Almeida,³ and Felipe F. Fanchini^{3,1,*}

¹*São Paulo State University (UNESP), School of Sciences, 17033-360 Bauru-SP, Brazil*

²*Instituto de Física Gleb Wataghin, Universidade de Campinas, Campinas, 13083-970, SP, Brazil*

³*Hospital Israelita Albert Einstein, São Paulo-SP, Brazil*

(Dated: February 25, 2026)

Reconstructing DNA sequences without a reference, known as *de novo* assembly, is a complex computational task involving the alignment of overlapping fragments. To address this problem, a usual strategy is to map the assembly to a Quadratic Unconstrained Binary Optimization (QUBO) formulation, which can be solved by different quantum algorithms. In this work, we focus on three versions of the Feedback-based Algorithm, a protocol that eliminates classical optimization loops via measurement feedback. We analyze long-read DNA fragments from SARS-CoV-2 and human mitochondrial DNA using standard FALQON, second-order FALQON (SO-FALQON), and time-rescaled FALQON (TR-FALQON). Numerical results show that both variants improve convergence to the ground state and increase success probabilities at reduced circuit depths. These findings indicate that enhanced feedback-driven dynamics are effective for solving combinatorial problems on near-term quantum hardware

I. INTRODUCTION

Genomic diversity is driven by complex events such as recombination, duplication, and transposition. While these mechanisms are essential for evolution, they render the genome computationally challenging to reconstruct. In biotechnology, the *de novo* reconstruction of genomes from high-throughput sequencing *reads* has become a critical step for the characterization of organisms without prior reference, as well as for metagenomic studies and clinical diagnostics [1]. These reads, typically hundreds of bases long, present partial overlaps that must be optimally aligned, a task complicated by genomic repetitions, sequencing errors, and the large volume of data, challenges that have led to classical solutions based on de Bruijn graphs [2], assembly heuristics such as Velvet, SPAdes, and ABySS [3, 4], which still face limitations of scalability and accuracy in large genomes.

High-fidelity genome assemblies enable fundamental applications in medicine and biology as identification of genetic variants associated with hereditary diseases, monitoring of infectious outbreaks through genomic surveillance, studies of molecular evolution, and the development of personalized therapies and regenerative medicine [5, 6]. In addition, fast and accurate assemblies reduce research costs and enable real-time analysis in critical clinical situations.

The formulation of the assembly problem as a *Travelling Salesman Problem* (TSP) on a graph whose edges represent negative overlap costs naturally leads to the QUBO (Quadratic Unconstrained Binary Optimization) expression, an approach that benefits from advances in quantum optimization and hybrid simulations [7–9]. An approach involving the QAOA (Quantum Approximate

Optimization Algorithm) algorithm has been previously carried out, making use of the QUBO formulation applied to DNA assembly [10].

The application of quantum computation to DNA reconstruction has been investigated in [11, 12] using quantum annealing and in [13] using pangenome method similar to graph-based formulation related to de Bruijn graph. Concurrently with the development of the present work, a closely related study proposed a quantum-assisted graph-optimization pipeline for *de novo* assembly, formulating Hamiltonian and Eulerian path problems on the assembly graph as a higher-order binary optimization (HOBQ) model solved with a gate-based VQE, and introducing a bitstring-recovery mechanism to improve exploration of the solution space [14]. This independent progress reinforces the timeliness of quantum-assisted formulations for assembly, while highlighting complementary directions: whereas that approach couples quantum optimization with classical pre-/post-processing, here we focus on feedback-driven quantum dynamics via FALQON and its variants, eliminating any classical parameter-optimization loop.

In present work, we propose employing the *Feedback-based Algorithm for Quantum Optimization* (FALQON), a purely quantum algorithm that uses measurement feedback to dynamically adjust the circuit parameters, eliminating any classical optimization step [15], as is commonly observed in NISQ (Noisy Intermediate Scale Quantum) processes [16]. To expand this approach, we also introduce two variants: the *Time-Rescaled FALQON* (TR-FALQON), which applies temporal rescaling to the circuit operators to accelerate convergence at shallow depths [17]; and the *Second-Order FALQON* (SO-FALQON), which modifies the feedback law by including a second-order approximation in the time interval, allowing larger steps and a significant reduction in circuit depth [18]. Both variants aim to overcome practical limitations of the original FALQON, especially in NISQ

* felipe.fanchini@unesp.br

devices with restricted circuit depth.

This paper is organized as follows: in Section II we discuss in detail the DNA assembly problem and its rigorous mapping to the QUBO/Ising formalism; in Section III we present the motivation, Lyapunov control, and functioning of the FALQON algorithm; in Section IV we describe the TR-FALQON variant, with emphasis on temporal rescaling techniques and their benefits for shallow circuits; Section V is dedicated to the formulation of SO-FALQON and the discussion of the second-order approximation; in Section VI we present the computational implementation of the methods and experiments; in Section VII we report and analyze the results obtained, comparing convergence rates, fidelity, and robustness of the different approaches; and finally, in Section VIII we discuss conclusions and perspectives for the work.

II. DNA DECODING PROBLEM VIA DE NOVO ASSEMBLY

De novo genome assembly aims to reconstruct a complete genomic sequence without the aid of a pre-existing reference, starting from small sequencing fragments generated by high-throughput sequencing platforms such as Illumina. Each read has a typical length that varies depending on the technology and may contain insertion, deletion, and substitution errors [6]. The coverage depth (the average number of times each genomic position is read) must be sufficient to guarantee redundancy but exponentially increases the data volume. Additionally, repetitive regions and structural variants create ambiguities that hinder exact assembly, requiring robust methods to distinguish real biological events from sequencing artifacts [2, 3].

A. Overlap–Layout–Consensus Model

In the overlap–layout–consensus paradigm, each sequencing fragment (read) r_i is represented by a vertex in a directed graph

$$G = (V, E), \quad V = \{r_1, r_2, \dots, r_N\}.$$

This model, introduced in Sanger fragment assemblies and refined for long reads of third-generation sequencing [19, 20], remains the basis of modern assemblers such as Canu and Flye [21, 22].

For each ordered pair (r_i, r_j) , the minimum overlap length required for the suffix of r_i to match the prefix of r_j is defined as [23],

$$\begin{aligned} \text{ov}(i, j) &= \max_{k \leq \min(|r_i|, |r_j|)} \left\{ \begin{array}{l} \text{suffix of } r_i \text{ of length } k \\ = \text{prefix of } r_j \text{ of length } k \end{array} \right\} \quad (1) \end{aligned}$$

and the adjacency matrix elements of this directed graph become,

$$w_{i,j} = -\text{ov}(i, j), \quad (2)$$

where more negative values correspond to larger overlaps and, therefore, greater assembly affinity [2, 10]. Note that, in general,

$$\text{ov}(i, j) \neq \text{ov}(j, i),$$

due to sequencing errors and differences in prefix versus suffix alignment [20].

The search for a minimum-cost Hamiltonian cycle in G aims to find an order of visiting all vertices that maximizes the sum of consecutive overlaps. This cycle arises because each vertex must be used exactly once, forming a loop that returns to the starting point or extending into a linear sequence, depending on the assembly strategy. In optimization terms, a Hamiltonian cycle corresponds to the solution that simultaneously satisfies the constraint of single use of each read and organizes the overlaps in a globally optimal manner [4, 19].

Simplified example: As an illustrative example, we use the following four reads, constructed as cyclic rotations of length 8 to guarantee nonzero overlaps for all pairs:

$$\begin{aligned} r_0 &= \text{ATCGATCG}, \\ r_1 &= \text{CGATCGAT}, \\ r_2 &= \text{TCGATCGA}, \\ r_3 &= \text{GATCGATC}. \end{aligned}$$

The overlap graph constructed from these four reads is presented in Fig. 1.

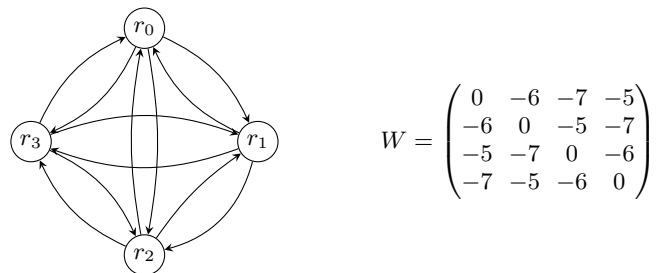


Figure 1. Directed complete graph constructed from four reads and its corresponding adjacency matrix. Each line(column) i, j , corresponds to the connectivity between reads r_i, r_j .

After identifying the minimum-cost Hamiltonian cycle, the *consensus* phase is applied, where each pair of overlapping reads is aligned according to the vertex sequence of the cycle, discrepancies are corrected by majority voting, and conflicts in repetitive regions are resolved based on coverage and quality [20]. The result is a reconstructed genomic sequence, free of reference bias and with global maximization of overlaps.

B. Problem Formulation as QUBO

The mapping of the de novo assembly problem to QUBO form allows its solution either by quantum annealing or by gate-based quantum algorithms such as variational or feedback-based methods [7, 8, 24]. This representation captures the combinatorial nature of the fragment reordering problem, formulating it as a quadratic energy minimization over binary variables subject to structural constraints.

Let N be the number of reads after preprocessing (redundancy removal, quality filtering, and chimera detection), we then introduce a binary variable $x_{i,p} \in \{0, 1\}$ indicating whether read r_i occupies position p in the final assembly:

$$x_{i,p} = \begin{cases} 1, & \text{if } r_i \text{ is at position } p, \\ 0, & \text{otherwise,} \end{cases} \quad i, p = 1, \dots, N.$$

The total QUBO objective function is represented as:

$$\min_{\mathbf{x} \in \{0,1\}^{N^2}} \mathbf{x}^\top Q \mathbf{x},$$

$$Q = A Q_{\text{pos}} + B Q_{\text{read}} + C Q_{\text{overlap}}, \quad (3)$$

where \mathbf{x} is a column matrix of binary variables $x_{i,p}$. Each component of eq. (3) is defined as it follows:

- **Position constraint:** Each position must contain exactly one read. The term penalizes any ambiguity or omission of allocation:

$$Q_{\text{pos}} = \sum_{p=0}^{N-1} \left(1 - \sum_{i=0}^{N-1} x_{i,p} \right)^2.$$

This term expands to generate quadratic and bilinear contributions that enforce uniqueness per position.

- **Uniqueness constraint:** The same read cannot occupy more than one position:

$$Q_{\text{read}} = \sum_{i=0}^{N-1} \left(1 - \sum_{p=0}^{N-1} x_{i,p} \right)^2.$$

This term also expands to penalize multiple occurrences of the same read.

- **Overlap cost:** For each consecutive pair of positions $(p, p+1)$, the cost is reduced by overlaps between reads,

$$Q_{\text{overlap}} = \sum_{p=0}^{N-2} \sum_{i=0}^{N-1} \sum_{\substack{j=0 \\ i \neq j}}^{N-1} w_{ij} x_{i,p} x_{j,p+1}.$$

The penalty coefficients A and B must satisfy:

$$A, B > \max_{i,j} |w_{ij}|,$$

so that no violation of constraints can be compensated by an overlap gain. However, values of A, B that are too large widen the spectral range of the Hamiltonian and hinder the solution process.

For quantum devices based on Pauli σ_z operators, such as those used in quantum annealing or in gate-based quantum algorithms it is necessary to convert the binary variables $x_{i,p} \in \{0, 1\}$ into spin variables $z_a \in \{-1, +1\}$. This conversion is carried out by the linear transformation,

$$x_{i,p} \rightarrow \frac{1 - z_a}{2}.$$

Substituting this relation into the quadratic objective function, we obtain:

$$\begin{aligned} \mathbf{x}^\top Q \mathbf{x} &= \left(\frac{1-z}{2} \right)^\top Q \left(\frac{1-z}{2} \right), \\ &= \frac{1}{4} z^\top J z - \frac{1}{2} h^\top z + \text{constant}, \end{aligned}$$

where the coefficients are defined as:

$$J_{ab} = 4Q_{ab}, \quad h_a = 2 \sum_b Q_{ab}.$$

The added constant does not affect the optimum position but is relevant for recovering the total energy. The final Hamiltonian in the Ising formalism takes the form:

$$H_{\text{Ising}} = \sum_{a < b} J_{ab} Z_a Z_b + \sum_a h_a Z_a,$$

where Z_a represents the Pauli σ_z operator acting on qubit a . This form is directly compatible with implementation in quantum hardware, allowing optimization algorithms to exploit the topology and physical limitations of the underlying architecture.

III. FALQON ALGORITHM

A. Motivation

In the context of DNA sequence assembly, the problem can be mapped into a QUBO model and subsequently transformed into an Ising Hamiltonian, as discussed in Sec. II B. Traditionally, variational algorithms such as the QAOA [25] apply parameterized circuits whose angles must be externally optimized by classical routines being computationally expensive procedure, especially in NISQ (Noisy Intermediate-Scale Quantum) architectures. In addition, the dependence on quantum-classical hybrid loops intensifies the impact of noise and limits scalability due to phenomena such as barren plateaus, in which parameter gradients become exponentially small with the number of qubits [26].

The FALQON algorithm [15] was proposed to overcome these limitations by using system measurements to dynamically update circuit parameters, completely eliminating the classical optimization loop. This strategy is grounded in quantum Lyapunov control techniques, which guarantee a monotonic descent trajectory of the expected energy value across circuit layers.

B. Formalism and Dynamics

Considering the Ising Hamiltonian already formulated to encode the DNA assembly problem,

$$H_p = \sum_{i < j} J_{ij} Z_i Z_j + \sum_i h_i Z_i,$$

FALQON employs as a driver Hamiltonian the transverse field term

$$H_d = \sum_{k=1}^n X_k, \quad (4)$$

where n is the number of qubits associated with the QUBO instance.

The system evolution is implemented through a sequence of alternating layers, applied according to the Trotter-Suzuki approximation:

$$|\psi_{k+1}\rangle = e^{-i\beta_k H_d \Delta t} e^{-iH_p \Delta t} |\psi_k\rangle,$$

where Δt is a fixed time step and β_k is the only parameter adjusted at each layer.

Unlike QAOA, the parameters β_k are not optimized by classical algorithms but dynamically updated through a feedback law based on the expectation value of the commutator between the Hamiltonians:

$$\beta_{k+1} = -i \langle \psi_k | [H_d, H_p] | \psi_k \rangle. \quad (5)$$

This procedure implements a Lyapunov control where

the feedback term enforces the time derivative of the expected energy $\langle H_p \rangle$ to be non positive, promoting a monotonic energy descent trajectory along the iterations [15].

C. Characteristics and Convergence

The FALQON protocol guarantees that, under regular conditions on the step size Δt , the expectation value of the energy $J_k = \langle \psi_k | H_p | \psi_k \rangle$ decreases with each applied layer, driving the system to progressively lower-energy states. The Lyapunov control implemented by feedback enables effective navigation of the solution space without the bottlenecks of a classical optimization loop.

In the context of DNA reconstruction, the application of FALQON makes it possible to search for optimal assembly configurations without relying on classical parameter optimization, making it suitable for noisy quantum architectures and medium-scale instances.

IV. TR-FALQON ALGORITHM

A. Temporal Rescaling and TR-FALQON Formalism

The *temporal rescaling* method redefines the evolution of physical time t in terms of a new parameter τ through the transformation $t = f(\tau)$, where $f(\tau)$ is a monotonically increasing function that satisfies $f(0) = 0$ and $f(\tau_f) = t_f$, and it is referred to as the temporal rescaling function [17]. By rewriting the dynamics in terms of τ ,

$$i \frac{d}{d\tau} |\psi(\tau)\rangle = H(f(\tau)) \dot{f}(\tau) |\psi(\tau)\rangle,$$

where $\dot{f}(\tau) = \frac{df(\tau)}{d\tau}$ and $\mathcal{H} = H(f(\tau)) \dot{f}(\tau)$ represents the rescaled Hamiltonian. The term $\dot{f}(\tau)$ acts as a dynamic scaling factor, when $\dot{f}(\tau) > 1$, the evolution is accelerated relative to physical time, while $\dot{f}(\tau) < 1$ slow down the evolution, allowing greater resolution in critical regions of the dynamics. Thus, rescaling directly controls the “rate” at which each part of the evolution occurs.

To implement this dynamics in a layer-based algorithm, the evolution is discretized into steps of size $\Delta\tau$ and the Trotter-Suzuki decomposition [27] is applied to approximate the evolution operator at each step. Each TR-FALQON layer takes the form:

$$|\psi_{k+1}\rangle = e^{-i\beta_k H_d \dot{f}(k\Delta\tau) \Delta t} e^{-iH_p \dot{f}(k\Delta\tau) \Delta t} |\psi_k\rangle,$$

where the factor $\dot{f}(k\Delta\tau)$ modifies the operators relative to the original FALQON.

The adaptation of the control parameters guarantees monotonic convergence of the energy and is given by

$$\beta_k = -\frac{1}{f(k\Delta\tau)} \langle \psi_{k-1} | i[H_d, H_p] | \psi_{k-1} \rangle. \quad (6)$$

Typical functions for $f(\tau)$ include polynomial and trigonometric forms [17].

B. Impact and Results

Numerical results show that TR-FALQON achieves high fidelities and convergence to optimal solutions with substantially smaller circuit depths compared to standard FALQON [17]. This is particularly relevant for DNA assembly in NISQ devices, where circuit depth and coherence time are practical limitations. In addition, the combination with variational techniques [16] and barren plateau reduction strategies [26] may further enhance the efficiency of the method in combinatorial problems.

V. SO-FALQON ALGORITHM

A. Mathematical Formalism

In SO-FALQON, the control parameter β_k is updated based on the condition that the expected value of the energy decreases with each new circuit layer,

$$\Delta \langle H_p \rangle_k = \langle H_p \rangle_k - \langle H_p \rangle_{k-1}.$$

To obtain this update, a second-order Taylor expansion of the evolution operators associated with H_p and H_d is performed. This expansion considers not only linear terms but also quadratic terms in β_k and Δt , resulting

$$\Delta \langle H_p \rangle_k \simeq \Delta t \beta_k A_{k-1} + (\Delta t)^2 \left[\frac{1}{2} \beta_k^2 B_{k-1} + \beta_k C_{k-1} \right], \quad (7)$$

where,

$$\begin{aligned} A_{k-1} &= i \langle \psi_{k-1} | [H_d, H_p] | \psi_{k-1} \rangle, \\ B_{k-1} &= \frac{1}{2} \langle \psi_{k-1} | [[H_d, H_p], H_d] | \psi_{k-1} \rangle, \\ C_{k-1} &= \langle \psi_{k-1} | [[H_d, H_p], H_p] | \psi_{k-1} \rangle. \end{aligned} \quad (8)$$

Minimizing expression (7) and initially assuming $B_{k-1} > 0$, we obtain

$$\beta_k = -\frac{2(A_{k-1} + \Delta t C_{k-1})}{\Delta t B_{k-1}}.$$

This choice guarantees that $\Delta \langle H_p \rangle_k < 0$. In the case where $B_{k-1} < 0$, in order to maintain the condition

$\Delta \langle H_p \rangle_k < 0$, the sign of B_{k-1} is inverted, resulting

$$\beta_k = -\frac{2(A_{k-1} + \Delta t C_{k-1})}{\Delta t |B_{k-1}|}. \quad (9)$$

In addition, it is common to impose bounds on the magnitude of β_k to ensure numerical stability and maintain the validity of the Taylor expansion used [18].

The circuit is built with layers implemented through the Trotter-Suzuki decomposition [27], such that each step applies the operators $e^{-i\beta_k H_d \Delta t}$ and $e^{-iH_p \Delta t}$, incorporating the second-order feedback in each iteration.

B. Practical Implementation and Results

SO-FALQON has been demonstrated numerically in problems such as MAX-CUT and ground-state preparation, showing a reduction in the circuit depth required for convergence compared to first-order FALQON [18]. In NISQ hardware, this advantage is significant, as it reduces susceptibility to noise and enables larger instances of combinatorial optimization, including DNA reconstruction formulated via QUBO/Ising [7].

VI. IMPLEMENTATION

The computational implementation of the proposed pipeline was carried out in Python, using a custom library developed in PyTorch [28], organized into modular stages, from DNA read preprocessing to the simulation and analysis of feedback-based quantum algorithms.

The starting point consists of reading and cleaning the DNA reads, followed by a systematic calculation of overlaps between each pair of reads, determining the largest suffix that coincides with the prefix of another read. This procedure is applied to all combinations of reads, constructing an overlap matrix (see Fig. 1) that will be used to define the weights in the QUBO Hamiltonian.

With the overlap matrix, the assembly problem is mapped into the QUBO form, becoming suitable to be solved by presented FALQONs algorithms.

A. Execution of Feedback-Based Algorithms

Three algorithms were implemented, FALQON, TR-FALQON, and SO-FALQON. The main aspects of each variant are presented below.

a. FALQON (First Order). In standard FALQON, the update of the control parameter β_k at each layer follows the first-order feedback rule described by Eq. (5).

b. TR-FALQON (Time-Rescaled FALQON). For TR-FALQON, the following temporal rescaling function

was adopted,

$$f(\tau) = a\tau - \frac{t_f}{2\pi a}(a-1) \sin\left(\frac{2\pi a}{t_f}\tau\right), \quad (10)$$

where a is the temporal contraction parameter, t_f is the final time, and τ represents the temporal variable associated with the layer. Owing to this choice, the temporal rescaling results in a contracted final time given by $\tau_f = t_f/a$. This function was chosen because it is the main one presented in the original work on the temporal rescaling method [29] and also the primary choice in the article introducing the TR-FALQON algorithm [17].

The rescaling factor $\hat{f}(\tau)$ is given by:

$$\hat{f}(\tau) = a - (a-1) \cos\left(\frac{2\pi a}{t_f}\tau\right). \quad (11)$$

At each layer k , the update of the control parameter is performed according to Eq. (6).

c. SO-FALQON (Second Order). In SO-FALQON, a hybrid approach was used for the update of β_k , computing both the first-order feedback rule $\beta^{(1)}$, described by Eq. (5), and the second-order feedback law $\beta^{(2)}$, described by Eq. (9).

After calculating both candidates for β_k , the algorithm selects between $\beta^{(1)}$ and $\beta^{(2)}$ according to the magnitude of each term,

$$\beta = \begin{cases} \beta^{(2)}, & \text{if } |\beta^{(1)}| > |\beta^{(2)}|; \\ \beta^{(1)}, & \text{otherwise.} \end{cases}$$

This adaptive choice allows SO-FALQON to combine the robustness of the second-order approximation with the stability of the first-order rule, resulting in efficient convergence even for relatively large time intervals, as detailed in [18].

B. Metrics, Visualization, and Reproducibility

At the end of the executions, the solutions are evaluated in terms of final energy, fidelity to the optimal assembly, and convergence. All functions are parameterized and documented, enabling the replication of experiments and the extension to new datasets or encoding strategies.

VII. RESULTS

The experiments were conducted to compare the performance of the FALQON, TR-FALQON, and SO-FALQON algorithms in DNA assembly considering 5 real reads of SARS-CoV-2.

We adopt long SARS-CoV-2 reads to obtain more informative and less ambiguous overlaps: longer sequences

reduce spurious matches and the degeneracy of the overlap scores, yielding a cleaner QUBO energy landscape while preserving the same qubit footprint (which depends on the number of reads, not on their length). This choice provides a biologically relevant benchmark where the assembly constraints are realistic, yet the encoded instance remains tractable.

To satisfy the *one-hot* constraint and ensure combinatorial feasibility, the QUBO Hamiltonian was constructed according to the formalism proposed by Lucas [7]. To reduce the number of required qubits, the read with index 0 in each set was fixed in the first position. In this way, the problem encoding requires $(n-1)^2$ qubits for n reads, resulting in 16 qubits for the set of 5 reads.

In all experiments, the initial state used was

$$|\psi_0\rangle = |+\rangle^{\otimes n}, \quad (12)$$

and the driver Hamiltonian adopted was

$$H_d = \sum_i X_i. \quad (13)$$

The numerical results are presented in Figure 2, where Fig. 2 (a) presents the expected value of H_p as a function of the number of layers. Fig 2 (b) shows the evolution of the control parameters β_k considering each algorithm along the layers. Fig 2 (c) presents the probability of measuring the solution state defined as $P_k = |\langle \text{solution} | \psi_k \rangle|^2$, from the produced state at each layer.

Each panel compares the results of FALQON with those obtained by TR-FALQON and SO-FALQON, considering two distinct sets of hyperparameters for both algorithms. The configurations using the first set are referred to as TR-FALQON 1 and SO-FALQON 1, respectively represented by the red and purple solid lines in Figure 2, while those using the second set are denoted as TR-FALQON 2 and SO-FALQON 2, corresponding respectively to the dashed red and purple lines. The hyperparameter sets used for TR-FALQON and SO-FALQON are not identical. The first set employs milder parameters, closer to those used in FALQON, whereas the second set adopts more aggressive values to promote faster convergence. All algorithms were run with up to 300 layers and in all cases, the algorithms converged to a state in which the solution corresponds to the ground state with the highest probability of being measured.

Comparing the energy convergence curves of the three methods, the TR-FALQON 1 achieve the lowest final energy, also achieving the highest probability over 50%. The TR-FALQON 2, SO-FALQON 1 and 2, show similar final energy values, however with distinct measurement probability. FALQON is just behind its variants. The TR-FALQON 2 converges to its minimum with the lowest number of layers, this energy value is achieved when the corresponding optimization parameter β_k tends to zero, where the probability saturates about 40%.

Overall, it can be observed that milder hyperparameter configurations lead to a smoother initial convergence,

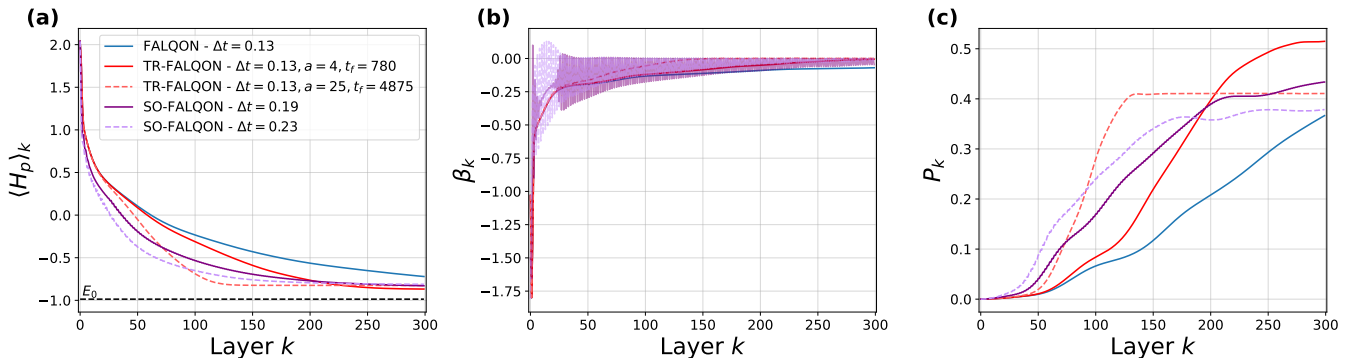


Figure 2. Performance of FALQON and its variants in the DNA assembly problem. The first panel shows the expected value of the energy $\langle H_p \rangle_k$ as a function of the circuit layer k . The second panel presents the values of the control function β_k . The third panel displays the probability P_k of measuring the state that encodes the optimal solution of the problem in each circuit layer. Each curve corresponds to a different variant of the algorithm, as indicated in the legend. The black dashed curve in the panels of the first row indicates the ground-state energy E_0 of H_p .

similar to FALQON, while more aggressive configurations result in a steeper initial drop followed by stagnation at higher energy levels. Furthermore, the advantage of the TR-FALQON and SO-FALQON variants becomes more pronounced as the number of reads increases, indicating better scalability of these methods for more complex instances.

In addition to the main SARS-CoV-2 instance, we carried out supplementary experiments with $n = \{4, 5, 6\}$ reads to probe how performance changes as the problem size increases. As n grows, the combinatorial search space expands (in principle scaling with $n!$ permutations), and the binary one-hot encoding requires $(n-1)^2$ qubits, so the underlying Hilbert space dimension grows as $2^{(n-1)^2}$, making the optimization landscape progressively more challenging. These additional benchmarks are important to assess scalability and robustness across distinct genomic sources, and their full results are reported in Appendix A.

VIII. CONCLUSION

In this work, we investigated the application of the FALQON algorithm and its variants TR-FALQON and SO-FALQON to the DNA assembly problem formulated in the QUBO/Ising formalism. The results show that, although the original FALQON ensures convergence and eliminates the need for classical optimization, its circuit depth still imposes practical limitations on NISQ devices.

The proposed variants demonstrated relevant advantages: TR-FALQON, by introducing temporal rescaling, achieved high success probabilities in shallow circuits, while SO-FALQON proved capable of maintaining robustness and stability even with larger time intervals, reducing the circuit depth required to reach high-quality solutions.

These results indicate that enhanced feedback strate-

gies, such as those incorporated in TR-FALQON and SO-FALQON, represent promising directions for feedback-based quantum computing in combinatorial problems. In particular, the fact that they require fewer layers makes these approaches more suitable for the current reality of NISQ processors, opening perspectives for the efficient application of feedback algorithms in larger-scale scenarios, such as complex genome assembly and other critical tasks in bioinformatics.

ACKNOWLEDGMENTS

G.S.F acknowledges support from Fundação de Amparo à Pesquisa do Estado de São Paulo (FAPESP), project number 2025/19585-6. P.M.P acknowledges support from Fundação de Amparo à Pesquisa do Estado de São Paulo (FAPESP), project number 2023/12110-7. L. A. M. Rattighieri acknowledges the support of Coordenação de Aperfeiçoamento de Pessoal de Nível Superior (CAPES), project number 88887.143168/2025-00. A. D. acknowledges support from Fundação de Amparo à Pesquisa do Estado de São Paulo (FAPESP), project number 2024/19054-8. F.F.F. acknowledges partial financial support from the National Institute of Science and Technology for Applied Quantum Computing through CNPq (Process No. 408884/2024-0) and from the São Paulo Research Foundation (FAPESP), through the Center for Research and Innovation on Smart and Quantum Materials (CRISQuaM, Process No. 2024/00998-6). We are grateful to Rodrigo Araújo Siqueira Barreiro and Gabriela Chiuffa Tunes of the AAMO group for helpful discussions.

Reads	Index	Sequence
4	0	ATGGCGTGCA
	1	GCGTGCAATG
	2	TGCAATGGCG
	3	AATGGCGTGC
5	0	ATGACCAACAACCTC
	1	AACAACCTCGGGCCC
	2	CTCGGGCCCTGACGC
	3	CCCTGACGCCTACGC
	4	GCCTACGCTCCTGGC
6	0	AGTGAAATTGACCTGCCCGTGAAGA
	1	CTGCCCCGTGAAGAGGCGGGCATAAC
	2	CGGGCATAACACAGCAAGACGAGAA
	3	ACAGCAAGACGAGAAGACCCTATGG
	4	AAGACCCTATGGAGCTTTAATTTAT
	5	TTTAATTTATTAATGCAAACAGTAC

Table I. Sets of reads used in the additional experiments (human mitochondrial reference genome, NC_012920.1) [30].

Appendix A: Additional Benchmarks: Human Mitochondrial Reads (4–6)

The experiments in this appendix compare the performance of FALQON, TR-FALQON, and SO-FALQON in DNA assembly using sets of 4, 5, and 6 real *reads* extracted from the human mitochondrial reference genome (NC_012920.1) [30]; the sequences are listed in Table I. To satisfy the *one-hot* constraint and ensure combinatorial feasibility, the QUBO Hamiltonian was constructed according to the formalism proposed by Lucas [7]. To reduce the number of required qubits, the read with index 0 in each set was fixed in the first position. In this way, the problem encoding requires $(n-1)^2$ qubits for n reads, resulting in 9, 16, and 25 qubits for the sets of 4, 5, and 6 reads, respectively.

In all experiments, the initial state used was

$$|\psi_0\rangle = |+\rangle^{\otimes n}, \quad (\text{A1})$$

and the driver Hamiltonian adopted was

$$H_d = \sum_i X_i. \quad (\text{A2})$$

The numerical results are presented in Fig. 3, organized into a grid of three rows by three columns (columns: 4, 5, and 6 reads). The first row shows the expected value $\langle H_p \rangle_k$ versus the number of layers, the second row shows the control parameters β_k across layers, and the third row shows the success probability

$$P_k = |\langle \text{solution} | \psi_k \rangle|^2, \quad (\text{A3})$$

computed from the state produced at each layer. Each panel compares FALQON with TR-FALQON and SO-FALQON (for two hyperparameter choices in the latter

methods). All algorithms were executed with up to 300 layers.

In the case of FALQON, the curves correspond to the time step that produced the largest energy decrease within the 300-layer limit. For 4 reads, this time step was below the critical step Δt_c (largest value that still guarantees monotonic convergence of the energy), since near Δt_c the algorithm exhibited stagnation in energy reduction. For 5 and 6 reads, no stagnation was observed, enabling the direct use of Δt_c .

Overall, the advanced feedback variants improve convergence and/or robustness under limited-depth regimes. These results align with recent analyses indicating that temporal rescaling (TR-FALQON) and second-order corrections (SO-FALQON) can accelerate convergence and increase the probability of obtaining the optimal solution [15, 17, 31], which is particularly relevant in NISQ settings where depth is constrained by noise and coherence time [32].

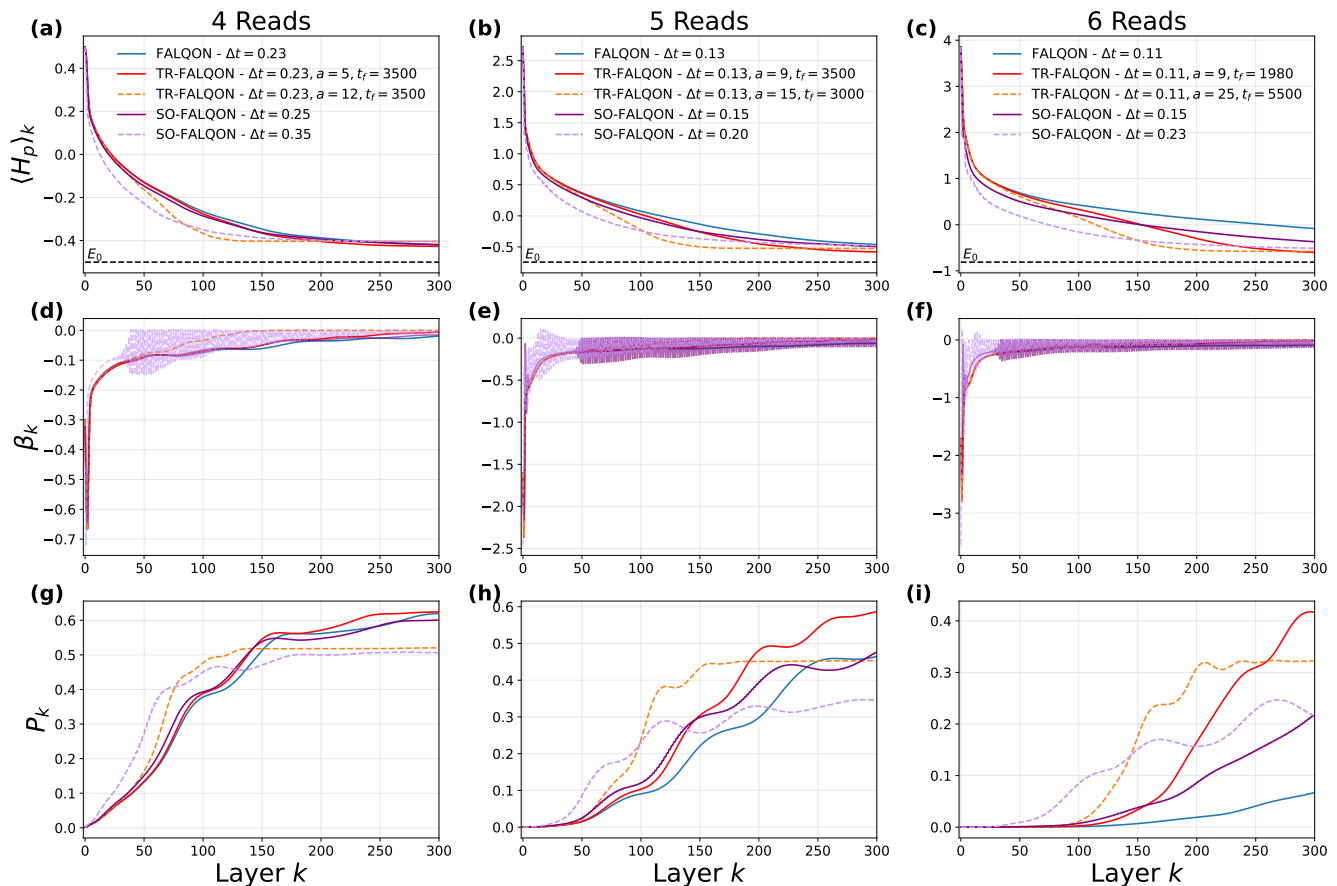


Figure 3. Performance of FALQON and its variants in the DNA assembly problem for instances with 4, 5, and 6 reads. The first row shows the expected value of the energy $\langle H_p \rangle_k$ as a function of the circuit layer k . The second row presents the values of the control function β_k . The third row displays the probability P_k of measuring the state that encodes the optimal solution in each circuit layer. Each curve corresponds to a different variant of the algorithm, as indicated in the legend. The black dashed curve in the panels of the first row indicates the ground-state energy E_0 of H_p .

-
- [1] J.-i. Sohn and J.-W. Nam, *Briefings in Bioinformatics* **19**, 23 (2016), <https://academic.oup.com/bib/article-pdf/19/1/23/25406900/bbw096.pdf>.
- [2] D. R. Zerbino and E. Birney, *Genome Research* **18**, 821 (2008).
- [3] A. Bankevich, S. Nurk, D. Antipov, A. A. Gurevich, M. Dvorkin, A. S. Kulikov, V. M. Lesin, S. I. Nikolenko, S. Pham, A. D. Prjibelski, *et al.*, *Journal of Computational Biology* **19**, 455 (2012).
- [4] J. T. Simpson, K. Wong, S. D. Jackman, J. E. Schein, S. J. M. Jones, and I. Birol, *Genome Research* **19**, 1117 (2009).
- [5] J. C. Venter, M. D. Adams, E. W. Myers, P. W. Li, R. J. Mural, G. G. Sutton, H. O. Smith, M. Yandell, C. A. Evans, R. A. Holt, *et al.*, *Science* **291**, 1304 (2001).
- [6] J. Shendure and H. Ji, *Nature Biotechnology* **26**, 1135 (2008).
- [7] A. Lucas, *Frontiers in Physics* **2**, 5 (2014).
- [8] F. Glover, G. A. Kochenberger, and Y. Du, arXiv preprint arXiv:1811.11538 (2018).
- [9] S. Jain, *Frontiers in Physics* **9**, 760783 (2021).
- [10] A. Sarkar, Z. Al-Ars, and K. Bertels, *PLOS ONE* **16**, e0249850 (2021).
- [11] K. Nałęcz-Charkiewicz and R. M. Nowak, *BMC Bioinformatics* **23**, 122 (2022).
- [12] A. S. Boev, A. S. Rakitko, S. R. Usmanov, A. N. Kobzeva, I. V. Popov, V. V. Ilinsky, E. O. Kiktenko, and A. K. Fedorov, *Scientific Reports* **11**, 13183 (2021).
- [13] J. Cudby, J. Bonfield, C. Zhou, R. Durbin, and S. Strelchuk, arXiv preprint arXiv:2508.08200 (2025).
- [14] J. V. Pamidimukkala, H. Sahu, A. Kannan, J. Ananthanarayanan, K. Dasgupta, and S. Senapati, *Accelerating de novo genome assembly via quantum-assisted graph optimization with bitstring recovery* (2026), arXiv:2602.00156 [quant-ph].
- [15] A. B. Magann, K. M. Rudinger, M. D. Grace, and M. Sarovar, *Physical Review Letters* **129**, 10.1103/PhysRevLett.129.250502 (2022).
- [16] M. Cerezo, A. Arrasmith, R. Babbush, S. C. Benjamin, S. Endo, K. Fujii, J. R. McClean, K. Mitarai, X. Yuan,

- L. Cincio, and P. J. Coles, *Nature Reviews Physics* **3**, 625 (2021).
- [17] L. A. M. Rattighieri, G. E. L. Peixe, B. L. Bernardo, and F. F. Fanchini, *Phys. Rev. A* **112**, 042607 (2025).
- [18] D. Arai, K. N. Okada, Y. Nakano, K. Mitarai, and K. Fujii, *Physical Review Research* **7**, 013035 (2025).
- [19] P. Pevzner, H. Tang, and M. Waterman, *Proceedings of the National Academy of Sciences* **98**, 9748 (2001).
- [20] E. Myers, *Bioinformatics* **21**, ii79 (2005).
- [21] K. Berlin, S. Koren, C.-S. Chin, *et al.*, *Nature Biotechnology* **33**, 623 (2015).
- [22] M. Kolmogorov, J. Yuan, Y. Lin, and P. A. Pevzner, *Nature Biotechnology* **37**, 540 (2019).
- [23] H. Li, *Bioinformatics* **32**, 2103 (2016).
- [24] V. Choi, *Quantum Information Processing* **7**, 193 (2008).
- [25] E. Farhi, J. Goldstone, and S. Gutmann, arXiv:1411.4028 (2014).
- [26] J. McClean, S. Boixo, V. Smelyanskiy, R. Babbush, and H. Neven, *Nature Communications* **9**, 4812 (2018).
- [27] M. Suzuki, *Physics Letters A* **146**, 319 (1990).
- [28] A. Paszke, S. Gross, F. Massa, A. Lerer, J. Bradbury, G. Chanan, T. Killeen, Z. Lin, N. Gimelshein, L. Antiga, *et al.*, *Advances in neural information processing systems* **32** (2019).
- [29] B. d. L. Bernardo, *Phys. Rev. Res.* **2**, 013133 (2020).
- [30] GenBank, *Homo sapiens mitochondrion, complete genome*, https://www.ncbi.nlm.nih.gov/nuccore/NC_012920.1 (2024), acessado em 2024-06.
- [31] D. Arai, K. N. Okada, Y. Nakano, K. Mitarai, and K. Fujii, arXiv preprint (2024), arXiv:2407.17810 [quant-ph].
- [32] J. Preskill, *Quantum* **2**, 79 (2018).